Sustainable Energy & Fuels

ROYAL SOCIETY OF CHEMISTRY

PAPER

View Article Online
View Journal | View Issue

Cite this: *Sustainable Energy Fuels*, 2020, **4**, 3388

A fundamental study of the thermoelectrochemistry of ferricyanide/ferrocyanide: cation, concentration, ratio, and heterogeneous and homogeneous electrocatalysis effects in thermogalvanic cells†

Mark A. Buckingham, ‡[a] Samer Hammoud,‡[a] Huanxin Li,[ab] Conor J. Beale,[a] Jason T. Sengel[a] and Leigh Aldous *[a]

Thermogalvanic cells typically utilise equimolar concentrations of the oxidised and reduced states of a redox couple in solution, sandwiched between two electrodes at dissimilar temperatures; entropy drives redox processes to occur at these electrodes, generating a potential difference and a current. However, significant gaps still exist in fundamental data and understanding of these 'thermocells'. In this study, thermocells based upon potassium ferricyanide, $K_3[Fe(CN)_6]$, and potassium ferrocyanide, $K_4[Fe(CN)_6]$, were investigated. The ratio of the oxidised and reduced states were systematically varied, and this had a significant effect upon the power produced; notably maximum power did not correspond to the equimolar ratio. A concentration study using equimolar ratios was also performed. Trends in the potential generated as a function of temperature (or 'Seebeck coefficient') were rationalised by the Nernst equation and Debye–Hückel theory. The trends in the current and the electrical power produced were successfully modelled using the Butler–Volmer equation. The effects of heterogeneous electrocatalysis were also explored (using platinum and two types of graphite) as well as homogeneous electrocatalysis, by the direct addition of alkali metal salts (as lithium, sodium, potassium, rubidium and caesium chlorides and sulphates). Clear trends were observed, and homogeneous and heterogeneous electrocatalysis had an additive effect when combined. Addition of CsCl was able to boost the maximum power output by upto *ca.* 80%, *via* both an increased Seebeck coefficient (through altered solvation) and through increased current (*via* homogeneous electrocatalysis of electron transfer). Finally, a limited economic comparison was performed, which highlights how the use of non-stoichiometric ratios of the redox couple could improve the cost-per-power value of the systems.

Received 16th March 2020
Accepted 18th May 2020

DOI: 10.1039/d0se00440e

rsc.li/sustainable-energy

1. Introduction

There is currently extensive interest in thermoelectrochemistry, or temperature-dependent electrochemistry.[1] A primary application of this is for thermogalvanic processes;[2–5] here two electrodes at dissimilar temperatures sharing a common redox active electrolyte can convert the temperature gradient directly into electrical current.[2,6] This comes about due to the temperature dependence of the electrode potential, which is directly related to the entropy difference, as expressed in eqn (1);[7]

$$S_e = \frac{\Delta V}{\Delta T} = \frac{\Delta S_{rc}}{nF} \quad (1)$$

where ΔV is the potential difference across the two electrodes, ΔT is the absolute temperature difference between the two electrodes, n the number of electrons transferred, F the Faraday constant and ΔS_{rc} is the entropy difference between the oxidised and reduced states of the redox couple. When applied to thermogalvanic systems, this is normally expressed as the Seebeck coefficient (S_e, mV K^{-1});[8,9] however, it should be noted that this thermogalvanic Seebeck coefficient is distinct from the classical thermoelectric Seebeck effect and associated Seebeck coefficient.[10]

Several thermogalvanic cells (or 'thermocells') have been reported, using a range of organic solvents,[11] ionic liquids,[12] aqueous electrolytes[7,13] or their mixtures.[12] Numerous redox couples have been investigated, including metal-based iron,[7,13] cobalt,[11] copper[14,15] and lithium systems,[16,17] and a wide variety of other systems including, but not limited to, ferrocene/

[a]*Department of Chemistry, Britannia House, King's College London, London, SE1 1DB, UK. E-mail: leigh.aldous@kcl.ac.uk*

[b]*State Key Laboratory for Chemo/Biosensing and Chemometrics, College of Chemistry and Chemical Engineering, Hunan University, Changsha, Hunan, 410082, China*

† Electronic supplementary information (ESI) available. See DOI: 10.1039/d0se00440e

‡ These authors contributed equally to this work.

ferrocenium[18,19] and I^-/I_3^-.[19–21] However, arguably the most extensively reported thermogalvanic system is aqueous $[Fe(CN)_6]^{3-/4-}$, or the ferricyanide/ferrocyanide redox couple.[6,13] This system has a relatively high S_e of *ca.* -1.4 mV K^{-1},[6] typically exhibiting fast, reversible electrode kinetics (as a *pseudo*-outer sphere redox couple),[22,23] and its potassium salts are relatively stable, soluble and commercially available.

The redox entropy of the $[Fe(CN)_6]^{3-/4-}$ redox couple has been reported to have an equivalent Seebeck of -1.8 mV K^{-1}, at low ionic strength values (<0.2 M).[24] However, typically the $[Fe(CN)_6]^{3-/4-}$-based thermogalvanic cells are formed by dissolving 0.2 M $K_3[Fe(CN)_6]$ and 0.2 M $K_4[Fe(CN)_6]$ in water, since this is near the solubility limits of the mixed system in water. At this higher ionic strength (3.2 M), a lower S_e value of *ca.* -1.4 mV K^{-1} is expected.[6] Higher concentrations have been reported, either where the cations are substituted for another cation such as $[NH_4]^+$ (up to 0.45 M of each redox state),[25] or for specialised high-temperature cells (up to 0.8 M of each redox state).[26] Typically the reduced and oxidised species are dissolved at matching concentrations, for obvious reasons; only one non-stoichiometric example for the thermoelectrochemistry of $[Fe(CN)_6]^{3-/4-}$ was found in the literature (employing 0.85 M $K_3[Fe(CN)_6]$ and 0.13 M $K_4[Fe(CN)_6]$) but the impact of using non-stoichiometric ratios was not discussed.[27]

Extensive work has explored the effect of altering the electrode, using the 0.2 M $K_3[Fe(CN)_6]$ and 0.2 M $K_4[Fe(CN)_6]$ system in water as a 'standard system'. Many of these systems have focussed upon modified carbon electrodes, mainly utilising carbon nanotubes,[25,28–32] where changes in the geometry and surface area are likely dominant. Others have used planar electrodes, including platinum,[6,33] stainless steel,[13] gold[34] and a range of carbon materials[25,35] such as carbon nanotubes,[36,37] reduced graphene oxide (rGO)[38] and carbon aerogels.[29] This has been observed to have significant electrocatalytic effects, with for example platinum-sputtered stainless steel generating orders of magnitude higher power than that of bare stainless steel.[33,39] Poisoning effects also need to be considered, *e.g.* a short term electrocatalytic effect was observed by introducing gold nanoparticles upon a carbon electrode, but over longer times this resulted in lower power output due to $[Fe(CN)_6]^{3-/4-}$-induced corrosion of the gold nanoparticles.[34] Stainless steel electrodes can have their electrocatalytic performance with respect to $[Fe(CN)_6]^{3-/4-}$-based thermogalvanic cells enhanced by acid treatment, or decreased by extended exposure to the $[Fe(CN)_6]^{3-/4-}$.[39]

Others have explored $[Fe(CN)_6]^{3-/4-}$-based thermogalvanic cells mixing water with organic solvents (such as methanol), and observed changes in the S_e associated with altered solvation spheres around the two redox states; early reports indicated it significantly increased the S_e,[40] whereas subsequent comprehensive work has demonstrated the opposite.[41] This was expanded by using 24 M urea and 2.6 M guanidine chloride as additives to 0.2 M $K_3[Fe(CN)_6]$ and 0.2 M $K_4[Fe(CN)_6]$ in water, to also improve the S_e to -4.2 mV K^{-1}.[42] Recently, the effect upon the ΔS_{rc} of the $[Fe(CN)_6]^{3-/4-}$ redox couple of a large excess of electrolyte has also been investigated.[43] It was observed that 'structure breaking ions' such as Cs^+ were found to increase the entropy change in the system, whereas 'structure-making ions' such as Li^+ were found to decrease the entropy change in the system.[43] Gelled aqueous electrolytes have also been investigated for $[Fe(CN)_6]^{3-/4-}$-based thermogalvanic cells, using cellulose,[44] sodium polyacrylate,[39] poly(vinyl alcohol)[45] and agar agar[39] as gelling systems.

As such, the addition of alkali metal cations to $[Fe(CN)_6]^{3-/4-}$-based systems can alter entropy changes in the system,[43] but this has not been explored in thermogalvanic cells. Additionally, no fundamental investigation has explored the effect of using non-stoichiometric ratios of the redox couple in thermogalvanic cells. Limited fundamental electrocatalytic work has also been performed. As such, here we report an in-depth study of the $[Fe(CN)_6]^{3-/4-}$ redox system in a thermoelectrochemical context, where the effect of $[Fe(CN)_6]^{3-/4-}$ concentration, the concentration ratio of $[Fe(CN)_6]^{3-}$: $[Fe(CN)_6]^{4-}$ ions and altering the counter-cation have been investigated with respect to the Seebeck coefficient, current density and power density in thermogalvanic cells. Significant trends were observed in the S_e and power output upon altering the ratio; this was rationalised and modelled based upon a combination of Nernstian and Butler–Volmer behaviour. Ultimately, a non-stoichiometric ratio (0.15 M $K_3[Fe(CN)_6]$ + 0.25 M $K_4[Fe(CN)_6]$) displayed slightly higher power output than the stoichiometric ratio (0.20 M $K_3[Fe(CN)_6]$ + 0.20 M $K_4[Fe(CN)_6]$). The effect of added alkali metal cations was also capable of boosting the thermogalvanic cells power output, representing a means of 'homogeneous electrocatalysis'. This was compared with conventional 'heterogeneous electrocatalysis' by varying the electrode material. Finally, a preliminary cost comparison of the $[Fe(CN)_6]^{3-/4-}$ thermocell demonstrated that although 'homogeneous electrocatalysis' using caesium chloride afforded the most powerful thermogalvanic cell, it was 7-fold higher on a cost of electrolyte-per-power output basis. Non-stoichiometric cells were in fact found to be the most economically favourable systems, demonstrating how a 'less is more' approach can be effective in thermogalvanic cells.

2. Experimental

2.1. Chemicals

All reagents were purchased from UK suppliers and were used as received, unless otherwise specified. These were potassium ferrocyanide ($K_4[Fe(CN)_6]$, potassium hexacyanoferrate(II) trihydrate, ≥99.5%, Sigma Aldrich), potassium ferricyanide ($K_3[Fe(CN)_6]$, potassium hexacyanoferrate(III), ≥99.0%, Sigma Aldrich), lithium chloride (Fluorochem), lithium sulphate (99%+, Acros Organics), sodium chloride (≥99.5%, Sigma Aldrich), sodium sulphate (≥99.0%, Sigma Aldrich), potassium chloride (≥99.0%, Sigma Aldrich), potassium sulphate (≥99.0%, Sigma Aldrich), rubidium chloride (Fluorochem), rubidium sulphate (99.8%, Sigma Aldrich), caesium chloride (Fluorochem) and caesium sulphate (99%, Alfa Aesar). All water used was ultra-purified, with a resistivity of 18.2 MΩ cm.

2.2. Thermoelectrochemical setup

One thermoelectrochemistry set-up was employed, employing two different thermoelectrochemical cells. Broadly, all electrodes were

placed in thermal contact with copper-based CPU cooling blocks (purchased from eBay.co.uk). These CPU copper heat exchangers had their temperature controlled by flowing water from two TX150-R2 heated/refrigerated thermostatic circulator baths (Grant Instruments Ltd, UK), to within <0.1 °C accuracy.

Two distinct cells were employed, as described below. During measurements the cell and electrodes were arranged horizontally, and vertically with respect to gravity.[14]

Throughout this study, a temperature difference (ΔT) of 20 °C was applied. This was achieved with 'hot' and 'cold' temperatures, T_{hot} and T_{cold}, of 35.0 °C and 15.0 °C, respectively. However, careful analysis revealed that although a ΔT of 20 °C was applied *via* the water, the electrodes experienced a ΔT value of *ca.* 18 °C. The lab was *ca.* 24 °C, and much of the temperature gradient was lost at the cold electrode, such that T_{cold} was actually *ca.* 17 °C. All reported S_e values have been corrected to reflect this.

2.2.1 Graphite thermoelectrochemical cell. The graphite electrodes utilised were either crystalline graphite (Pyrolytic Graphite Thermal Interface Material, 0.05 mm thick, RS Components Ltd, UK) or amorphous graphite (99.5% pure graphite gasket foil, 1 mm thick, Xiaochengshop, China).

All graphite electrode measurements were performed using a thermoelectrochemical cell (shown in Fig. 1) that consisted of a nylon 6,6 cylinder with an outer diameter of 18 mm, an inner diameter of 8 mm and a length of 8 mm (RS Components Ltd, UK). This was placed between two graphite electrodes, which were held in contact with the copper heat exchangers *via* silicone heat transfer compound (Pro-Power, RS Components Ltd, UK). The contact area between the solution and the electrode was fixed by covering the graphite with an adhesive polyethylene label (P12/64 R MWPE, Label Planet, UK) into which a 6 mm diameter hole had been punched; this gave a consistent geometric electrode surface area of 28 mm^2, with an inter-electrode spacing of 8 mm.

2.2.2 Platinum thermoelectrochemical cell. All platinum measurements were performed using a tailor made poly(methyl methacrylate) (PMMA) cell, made in-house. CAD drawings of the cell was made using SolidWorks 2006 SP4.1, and prepared on a Roland MDX-40 CNC (computer numerical control) vertical milling machine using 1–3 mm square end mills. First, the rectangular cell was machined from cast PMMA, measuring 30 mm (width) × 20 mm (height) × 8.4 mm (depth). Subsequently, a 6.7 mm diameter cylinder was formed (through the 8.4 mm deep section); a 10 mm diameter lip (0.5 mm deep) was then machined at each opening. Two smaller holes were drilled to allow direct injection of the electrolyte into the transparent PMMA cell. Solid platinum discs were placed in each lip as electrodes (1 mm thick with 10 mm diameter, from Surepure Chemetals, USA). This gave a consistent geometric electrode surface area of 35 mm^2, with an inter-electrode spacing of 7.4 mm. The electrodes were held in place by copper tape, which was then placed in contact with the copper heat exchangers, which had been covered in a layer of crystalline graphite (Pyrolytic Graphite Thermal Interface Material, 0.05 mm thick, RS Components Ltd, UK).

2.2.3 Thermogalvanic power characterisation. The characterisation of the thermogalvanic cells was performed using a Keysight B2901A Source Measure Unit (Keysight, UK) and Quick IV software, following the 'sequence of constant voltages' method outlined in detail elsewhere.[10]

2.3. Thermogalvanic concentration and ratio study of $K_3[Fe(CN)_6]$ and $K_4[Fe(CN)_6]$

These thermogalvanic measurements were performed using the graphite thermoelectrochemical cell mentioned above, using the amorphous graphite electrodes. The concentration study used a series of concentrations comprising equimolar amounts of both $K_3[Fe(CN)_6]$ and $K_4[Fe(CN)_6]$ in water, using 0.05 M, 0.1 M, 0.15 M, 0.2 M or 0.25 M of each. The latter solution was essentially super-saturated; all were prepared freshly prior to measurement.

The ratio study used a series of concentrations with different ratios of $K_3[Fe(CN)_6]$ and $K_4[Fe(CN)_6]$ in water, where the sum of the concentrations of $K_3[Fe(CN)_6]$ and $K_4[Fe(CN)_6]$ always added up to 0.4 M. Therefore solutions were prepared which contained $K_3[Fe(CN)_6]$ at concentrations of 0 M, 0.025 M, 0.05 M, 0.1 M,

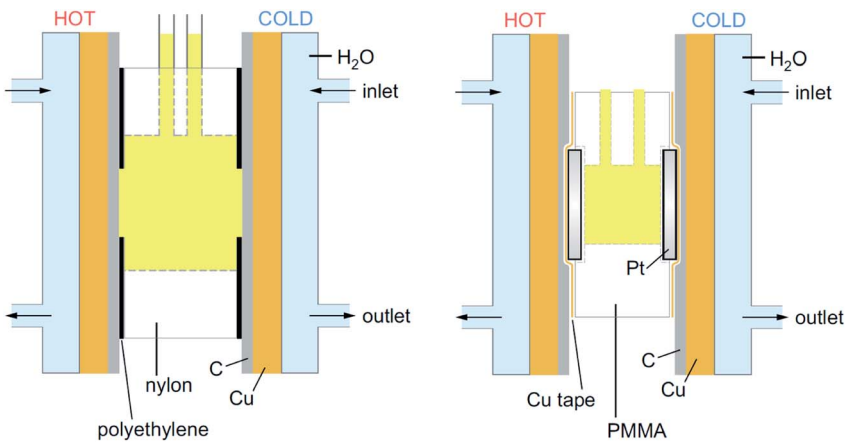

Fig. 1 Schematic representation of the two thermocells employed in this report (approximately to scale), where (left) the cell is nylon-based and employed with graphite electrodes (denoted by C), and (right) the cell is PMMA-based and employed with platinum electrodes (Pt). Both were temperature-controlled by copper (Cu) heat-exchangers in direct contact with thermostatic water (H_2O) *via* the indicated inlets and outlets.

0.15 M, 0.2 M, 0.25 M, 0.3 M, 0.35 M, 0.375 M and 0.4 M, with the concentration of $K_4[Fe(CN)_6]$ in the system following the reverse order.

2.4. Alkali metal cation effect upon the thermoelectrochemical properties of $[Fe(CN)_6]^{3-/4-}$

Studies were performed with added alkali metal salts. The Seebeck coefficients were initially determined in the platinum thermoelectrochemical cell mentioned above, using 5 mM $K_3[Fe(CN)_6]$ and 5 mM $K_4[Fe(CN)_6]$ and either 0.4 M X_2SO_4 or 1 M XCl, where X represents either the Li, Na, K, Rb or Cs salt. The ratio of X^+ to K^+ for X_2SO_4 and XCl was 23 : 1 and 29 : 1, respectively. The power density measurements were determined using the platinum cell, using 25 mM $K_3[Fe(CN)_6]$ and 25 mM $K_4[Fe(CN)_6]$ in the presence of 1.5 M XCl, where X represents either the Li, K or Cs salt. The ratio of X^+ to K^+ for these power measurements was 9 : 1. Finally, 200 mM $K_3[Fe(CN)_6]$ and 200 mM $K_4[Fe(CN)_6]$ were studied in both the graphite and the platinum cells, in the presence and absence of 0.7 M CsCl; here the ratio of Cs^+ to K^+ was 1 : 2.

2.5. Cyclic voltammetric study of alkali metal cation effect upon $[Fe(CN)_6]^{3-/4-}$

Cyclic voltammetric experiments were carried out using a PGSTAT204 potentiostat and NOVA 2.0 software (Metrohm Autolab, the Netherlands). The three-electrode experimental setup was a 1.6 mm diameter Pt disc electrode, a Pt wire counter electrode and an Ag/AgCl (3 M NaCl) reference electrode (all BASi, USA). All data was recorded at a scan rate of 50 mV s^{-1}. All solutions contained 5 mM $K_3[Fe(CN)_6]$ and 5 mM $K_4[Fe(CN)_6]$, with 0.4 M X_2SO_4 as supporting electrolyte, where X represents either Li, Na, K, Rb or Cs salt. The ratio of X^+ to K^+ was 23 : 1.

3. Results and discussion

3.1. Fundamental aspects of the thermogalvanic cell: concentration and ratio effects

3.1.1 The effect of the $K_{3/4}[Fe(CN)_6]$ concentration upon the thermogalvanic cell output. Some limited studies have investigated the effect of the overall concentration of equimolar $K_{3/4}[Fe(CN)_6]$ upon the performance of thermogalvanic cells; typically the short circuit current density (j_{sc}) and maximum power output (P_{max}) increased in an essentially linear manner with concentration.[6,25,30] The effect of the concentration upon the potential difference generated from the two electrodes as a function of the temperature difference (referred here to as the apparent Seebeck coefficient, S_e) was either not noted[6,25] or decreased slightly with increasing concentration.[30]

Here, an amorphous graphite electrode-based thermogalvanic cell was utilised, and the concentration of $K_3[Fe(CN)_6]$ and $K_4[Fe(CN)_6]$ were varied from a total concentration of 0.1 M (0.05 M of each) to 0.5 M (0.25 M of each). Fig. 2 displays the effect of altering concentration upon the (a) S_e, (b) j_{sc} and (c) P_{max}. The expected trends were observed, *i.e.* j_{sc} and P_{max} increased in an essentially linear manner with concentration, and the Seebeck coefficient decreased with increasing concentration; the latter observation is rationalised in terms of increasing ionic strength, and discussed further below. The relatively large uncertainties in the 0.25 M samples correspond to these solutions being essentially super-saturated, resulting in limited stability and relatively variable performance.

3.1.2 Study into the effect of the $K_3[Fe(CN)_6]$: $K_4[Fe(CN)_6]$ ratio upon the thermogalvanic cell. To the best of our knowledge, a systematic study of the effect of the ratio of $K_3[Fe(CN)_6]$ to $K_4[Fe(CN)_6]$ in a thermogalvanic cell has not been reported. Overwhelmingly, studies simply use them in an equimolar ratio. Ikeshoji investigated 0.85 M $K_3[Fe(CN)_6]$ and 0.13 M $K_4[Fe(CN)_6]$ (a ratio of 6.5 : 1), likely on account of the significantly higher solubility of the former, but the effect of using a non-stoichiometric ratio was not discussed.[27] The motivation for this study was two-fold; (i) the relative prices of $K_3[Fe(CN)_6]$ to $K_4[Fe(CN)_6]$ can vary significantly, and (ii) curiosity.

This study was performed by ensuring that the concentration of $K_3[Fe(CN)_6]$ plus that of $K_4[Fe(CN)_6]$ equalled 0.4 M, then varying the ratio of $[Fe(CN)_6]^{3-}$: $[Fe(CN)_6]^{4-}$. The results from these cells are summarised in Fig. 3, for (a) S_e, (b) j_{sc} and (c) P_{max}. Notably, here the S_e value varied significantly (between −1.65 mV K^{-1} and −1.22 mV K^{-1}).

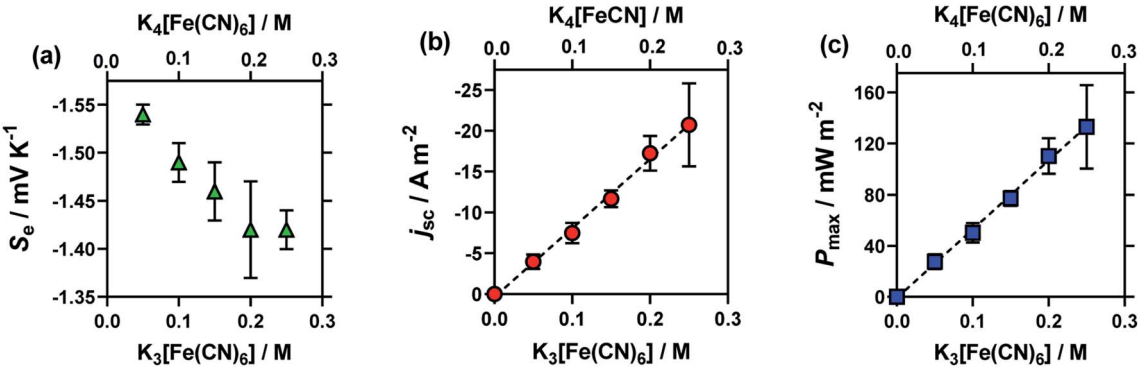

Fig. 2 Plots (a)–(c) showing the effect of the total concentration of equimolar $K_3[Fe(CN)_6]|K_4[Fe(CN)_6]$ upon (a) the S_e coefficient (green triangles), (b) the j_{sc} (orange circles) and (c) the P_{max} (blue square) of the thermocell. Obtained using the graphite thermocell using amorphous graphite electrodes, with applied $\Delta T = 18\,^{\circ}C$ ($T_{cold} = 17\,^{\circ}C$; $T_{hot} = 35\,^{\circ}C$), where error bars represent 1 SD from triplicate measurements. All values shown in these figures and other figures are tabulated in the ESI.†

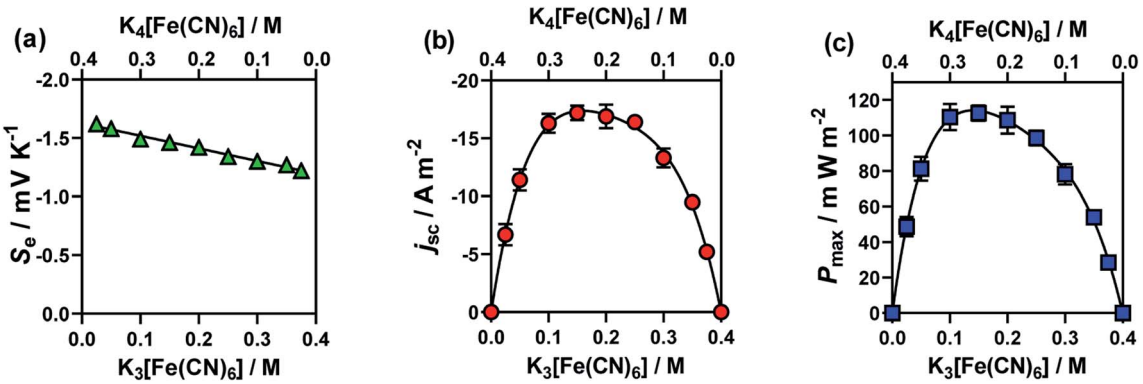

Fig. 3 Plots (a)–(c) showing the effect of changing the ratio of $[Fe(CN)_6]^{3-}$ to $[Fe(CN)_6]^{4-}$ upon (a) the S_e coefficient (green triangles); (b) the j_{sc} (orange circles) and (c) the P_{max} (blue squares). The concentrations of the redox couples were varied whilst maintaining a summed concentration of 0.4 M, where error bars represent 1 SD (not shown if bars smaller than symbol). All other experimental conditions as per Fig. 1.

The j_{sc} (Fig. 3(b)) displayed a polynomial-like relationship, with the highest current, in the region of 0.1–0.2 M $[Fe(CN)_6]^{3-}$ and 0.3–0.2 M $[Fe(CN)_6]^{4-}$. Notably, if this system was exclusively limited by the least abundant redox couple then an inverted V shape, Λ, would be expected, based upon the above concentration study. This more complex trend is quantitatively modelled and explained below.

The S_e was significantly higher in systems with more $[Fe(CN)_6]^{4-}$ than $[Fe(CN)_6]^{3-}$ (Fig. 3(a)); since a larger S_e typically results in a higher current, there is a slight asymmetry in the j_{sc} curve (Fig. 3(b)) towards the $[Fe(CN)_6]^{4-}$-rich systems. As the P_{max} is achieved at $0.5S_e$ and $0.5j_{sc}$, this asymmetry is even more significant in the power output (Fig. 3(c)), so much so that the cell containing 0.15 M $[Fe(CN)_6]^{3-}$ (a $[Fe(CN)_6]^{3-}$: $[Fe(CN)_6]^{4-}$ ratio of 3 : 5) generated the highest average P_{max} value. While this represents only a modest 4% increase, prior to now the general convention has been to always use a ratio of 1 : 1, or even the opposite ratio (significantly more $[Fe(CN)_6]^{3-}$).

3.1.3 Modelling the observed trends in the Seebeck coefficients. Changes in the S_e associated with changes in the concentration of redox couples have been previously related to changes in the ionic strength, and therefore can be attributed to a Debye–Hückel-like relationship[16,30,46,47] (providing they do not undergo other significant processes, such as hydrolysis[47]). The simplest possible representation of this is the Debye–Hückel limiting law;§

$$\ln(\gamma) = -Az_i^2 I^{0.5} \quad (2)$$

where γ is the activity coefficient, A is a constant that depends on temperature, z the charge number of the ionic species, and I the ionic strength of the solution. Assuming that the S_e is directly proportional to γ, this relationship can be simplified to;

$$\ln|S_e| \propto -I^{0.5} \quad (3)$$

§ This relationship can break down at higher I values, such that the γ can actually begin to increase with I; however, literature values for $[Fe(CN)_6]^{3-}$ and $[Fe(CN)_6]^{4-}$ do not demonstrate this characteristic change, which would require use of the extended Debye–Hückel law.

Broadly, such a relationship can be observed for the S_e trend *vs.* equimolar $[Fe(CN)_6]^{3-/4-}$ shown in Fig. 2(a); Fig. 4 displays this data re-plotted as $\ln(|S_e|)$ *vs.* $I^{0.5}$, and clearly demonstrated a linear correlation between the measured $\ln(|S_e|)$ and the $I^{0.5}$ of the relevant solution (●). Kang *et al.*[30] have previously varied the concentration of equimolar $K_{3/4}[Fe(CN)_6]$, applied 'Debye–Hückel treatment' and demonstrated a linear relationship between the S_e and the square root of concentration, $C^{0.5}$, but this only applied at extremely dilute concentrations; notably, they used S_e rather than $\ln|S_e|$, which likely explains this observation.

Fig. 4 also displays the data from the ratio study (■). The non-equimolar ratio system covers a systematic range of $I^{0.5}$ values, from 0.4 M $K_3[Fe(CN)_6]$ with an ionic strength of *ca.* 2.4 M, to 0.4 M $K_4[Fe(CN)_6]$ with an ionic strength of *ca.* 4 M. However, the trend of $\ln|S_e|$ *vs.* $-I^{0.5}$ from the ratio study (■) is clearly the opposite of that demonstrated by the concentration-study (●), intersecting only at the equimolar ratio. Therefore the Debye–Hückel relationship does not dominate in these systems. The electrochemical behaviour of non-equimolar concentrations of reduced and oxidised systems relative to

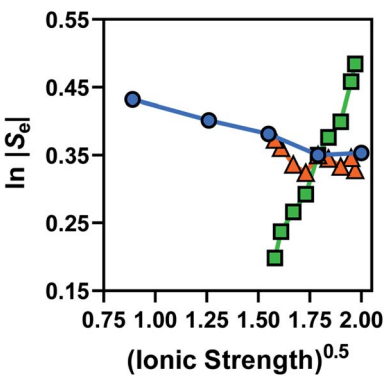

Fig. 4 Plots of the measured $\ln|S_e|$ *vs.* the (ionic strength)$^{0.5}$ of that particular solution, for the concentration study of equimolar $[Fe(CN)_6]^{3-/4-}$ (blue circles), non-equimolar concentrations of $[Fe(CN)_6]^{3-}$ to $[Fe(CN)_6]^{4-}$ (green squares) and the 'Nernstian corrected' form of the non-equimolar data to yield 'S_e^*' (red triangles).

equimolar systems is instead well described by the Nernst equation;

$$E_{\text{cell}} = E^{\circ}_{\text{cell}} - \frac{RT}{nF}\ln\left[\frac{C_{\text{red}}}{C_{\text{ox}}}\right] \quad (4)$$

where E_{cell} is the cell potential, E°_{cell} is the standard cell potential, n is the number of electrons transferred, R is the universal gas constant, T is the temperature, F is Faraday's constant, and C_{red} and C_{ox} are the concentrations of the reduced and oxidised species, respectively. By substituting E for ΔE, and T for ΔT then dividing by ΔT to obtain S_e rather than E, eqn (5) is obtained:

$$S_{e(\text{cell})} = S^{*}_{e(\text{cell})} - \frac{R}{nF}\ln\left[\frac{C_{\text{red}}}{C_{\text{ox}}}\right] \quad (5)$$

where $S^{*}_{e(\text{cell})}$ represents the S_e when the concentrations of both redox species are equal (*i.e.* $S^{*}_{e(\text{cell})} = -1.43$ mV K^{-1} when $[[Fe(CN)_6]^{3-}] + [[Fe(CN)_6]^{4-}] = 0.4$ M and $[[Fe(CN)_6]^{3-}] = [[Fe(CN)_6]^{4-}]$).[25,30] Thus $S_{e(\text{cell})}$ represents the S_e when the concentrations of the reduced and oxidised species are not equal.

Using eqn (5), the recorded S_e values for the non-stoichiometric systems shown in Fig. 3(a) were given a 'Nernstian correction' (*i.e.* converted from $S_{e(\text{cell})}$ into $S^{*}_{e(\text{cell})}$ using the known C_{red} and C_{ox} values). The Nernstian-corrected S^{*}_{e} values are also shown in Fig. 4 (▲), and the resulting $\ln|S^{*}_{e}|$ *vs.* $I^{0.5}$ displays the same Debye–Hückel-like relationship as that demonstrated by the concentration study (●). Therefore, the concentration imbalance is the main factor dictating the variation in S_e in the non-stoichiometric ratio study, in line with the Nernst equation, with the Debye–Hückel effect being a minor and opposite factor.

3.1.4 Modelling the power output from the ratio study: the dominating effect of Butler–Volmer kinetics. Whereas the equimolar concentration study demonstrated a clear linear relationship between concentration and current (Fig. 2(b) and (c)), the non-equimolar system displayed a characteristic polynomial-like relationship (Fig. 3(b) and (c)). In attempting to model this using a range of known electrochemical models, the Butler–Volmer equation was found to be a near ideal fit. The Butler–Volmer equation is widely used to rationalise or predict the current density, j, as a function of overpotential with the exchange current density, j_0, being a key parameter,[48] such that

$$j = j_0\left\{\exp\left[\frac{\alpha_a nF\eta}{RT}\right] - \exp\left[-\frac{\alpha_c nF\eta}{RT}\right]\right\} \quad (6)$$

$$j_0 = Fk^0(C_{\text{ox}}{}^{\alpha}C_{\text{red}}{}^{\alpha}) \quad (7)$$

where j is the measured electrode current density, j_0 is the exchange current density, α_a and α_c are the anodic and cathodic charge transfer coefficients, respectively, n is the number of electrons transferred, F is Faraday's constant, η is the activation over-potential, R is the universal gas constant, T is the temperature, k^0 is the electron transfer constant, and C_{ox} and C_{red} are the concentration of oxidised and reduced species, respectively. This was then adjusted to express the short circuit current density, j_{sc}, of the thermoelectrochemical systems, such that

$$j_{sc} = k_{agg}F\left(C_{\text{ox}}{}^{\alpha}C_{\text{red}}{}^{\alpha}\right)\left\{\exp\left[\frac{0.5V_{OCP}\alpha_a nF}{RT_{\text{cold}}}\right] - \exp\left[-\frac{0.5V_{OCP}\alpha_a nF}{RT_{\text{cold}}}\right]\right\} \quad (8)$$

where the overpotential has been expressed as $\eta = 0.5V_{OCP}$ (in Volts), T was set as the T_{cold} (known temperature of the cold electrode, 17 °C; assumed to be kinetically limiting), F and R are known constants, and C and n are both experimentally known. The charge transfer coefficients are known to be generally $\alpha_a = \alpha_c = 0.5$ for the $Fe(CN)_6]^{3-/4-}$ redox couple,[22] and thus were fixed as such. The results in a single unknown, k^0, which was reattributed as an aggregated rate constant, k_{agg} (for reasons described below). This also affords the P_{max}, by

$$P_{max} = 0.25 j_{sc} V_{OCP} \quad (9)$$

Fig. 5 displays the original j_{sc} and P_{max} data from the non-stoichiometric ratio study (from Fig. 3(b) and (c), respectively), but now overlaid with data generated from eqn (8) and (9), respectively, where the single unknown in the equation, k_{agg}, has been set as 1.68×10^{-4} cm s^{-1}. As can be observed,

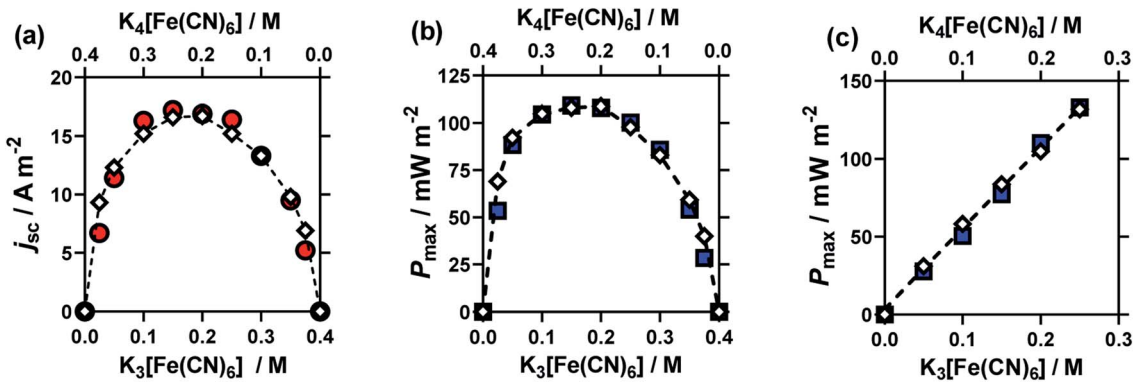

Fig. 5 Plots overlaying the experimental data points (coloured circles and squares) with Butler–Volmer modelled data points (white diamonds), for the non-equimolar ratio study, for (a) the j_{sc} and (b) P_{max}. Also shown in (c) are the experimental and modelled P_{max} data for the equimolar concentration study. All modelled data used $k_{agg} = 1.68 \times 10^{-4}$ cm s^{-1}, with all other parameters matching experimental conditions.

excellent correlation is observed between the experimental and modelled data, given that only a single parameter was varied.

A range of k^0 values are available in the literature for the $[Fe(CN)_6]^{3-/4-}$ redox couple, and typically range from *ca.* 0.020–0.25 cm s^{-1}.[22,49,50] However, this means the observed rate constant, k_{agg} of 1.68×10^{-4} cm s^{-1} is *ca.* 2 to 3 orders of magnitude lower than k^0 values; this is despite the amorphous graphite electrode material demonstrating excellent electrocatalytic ability, on par with platinum (discussed later). Here it must be recalled that the j_{sc} value is the steady state current achieved after the cell has been generating maximum current and therefore the concentration of redox active species at the electrode surface no longer matches that in the bulk. Modifications to the Butler–Volmer equation can introduce a ratio C^*/C_o, where C^* is the concentration at the electrode surface and C_o is the bulk concentration.[48] The C^* was therefore estimated using the Nernst equation, but when this correction was applied to the above model, it predicted that the cell would proceed in the opposite direction. The fact that this is not the case reflects that as the concentration ratio of the redox species varies, so does the overpotential (by virtue of the S_e changing). Therefore, a significantly more complicated system is required to model the cell when thermogalvanic current is generated; all forms of mass transport (diffusion, migration and convection) would need to be considered to determine concentration gradients, and then this needs to be used to account for how the overpotential is then changed as local concentration ratios and ionic strengths are altered at the electrode surface *via* redox processes.

Previously, Hornut and Storck stated that a Butler–Volmer equation-based model was in excellent agreement with experimental results from an equimolar $K_{3/4}[Fe(CN)_6]$ thermogalvanic cell (in 1 M NaOH); the Butler–Volmer equation was merged with a global mass transfer coefficient, and treated for ohmic drop.[51] However, comparison between experimental and modelled values appear to have been limited to a single experimental data point, and the values of the numerous specific parameters used in the substantial equation were unfortunately not stated. At present, we are not able to confidently formulate a complete model. However, it is remarkable that one of the simplest versions of the Butler–Volmer equation can be applied, and all kinetic, mass transport, overpotential and ohmic issues appear to be incorporated within a single constant, k_{agg}, as shown in eqn (8). While this k_{agg} cannot be taken as a universal constant (*e.g.* it is expected to include significant aspects of the cell geometry, including inter-electrode spacing, convection and be extremely ΔT sensitive) this could be utilised to compare different systems in the same cell. It also fully rationalises the observed polynomial-like dependence of the thermogalvanic output as a function of the ratio of [reduced] : [oxidised].

Finally, if this model is valid, it should be able to mirror the equimolar concentration results presented previously (*cf.* Fig. 2). Therefore the values from this study were applied to eqn (8), and the modelled data generated; the experimental data is overlaid *vs.* the experimental data in Fig. 5(c). As can be seen, excellent correlation is observed, using the same value of $k_{agg} = 1.68 \times 10^{-4}$ cm s^{-1}, as for the ratio study.

3.2. Homogeneous electrocatalysis effects in the thermogalvanic cell using cations

The rate constant of the $[Fe(CN)_6]^{3-/4-}$ redox system is known to be sensitive to both the electrode material[23,33,39] and to the cations[43,52,53] present in the system. Following on from the concentration and ratio study, the cation effect upon the thermogalvanic properties of the $[Fe(CN)_6]^{3-/4-}$ redox couple was explored. This was largely inspired by a recent publication by Huang *et al.*,[43] where they investigated the cation effect upon the (thermo)electrochemical properties (*i.e.* E°, S_e, k^0), but did not investigate the effect upon the thermogalvanic power (*e.g.* j_{sc} and P_{max}).

3.2.1 Cation effect upon the $E_{1/2}$ of the $[Fe(CN)_6]^{3-}$/$[Fe(CN)_6]^{4-}$ redox couple. As noted above, the $[Fe(CN)_6]^{3-/4-}$ redox system has been extensively investigated, both in terms of its electrochemistry and its thermoelectrochemistry, predominately as $K_3[Fe(CN)_6]$ and $K_4[Fe(CN)_6]$.[6,13] Initially, the cation effect was reinvestigated by the cyclic voltammetry (CV) of 5 mM $K_3[Fe(CN)_6]$ and 5 mM $K_4[Fe(CN)_6]$ in the presence of 0.4 M M_2SO_4 (where M = Li^+, Na^+, K^+, Rb^+ or Cs^+), using a platinum electrode in a standard 3-electrode cell. Here, the ratio of M^+ with respect to K^+ in the system was *ca.* 23 : 1.

The CVs for Li^+, K^+ and Cs^+ are displayed in Fig. 6(a), and the shift in $E_{1/2}$ for $[Fe(CN)_6]^{3-/4-}$ *vs.* the various M_2SO_4 salts are plotted in Fig. 6(b). Clearly, the different M^+ employed had a significant effect upon the $E_{1/2}$ values for the $[Fe(CN)_6]^{3-/4-}$ couple. This could potentially correspond to a junction potential between the electrolyte and the Ag/AgCl reference electrode; however, these observations are consistent with several other electrochemical studies, which have observed the strong effect that alkali metal cations have upon the properties of the $[Fe(CN)_6]^{3-/4-}$ redox couple.[43,52,53] This effect is also prevalent in solution, such as the homogeneous electron exchange reactions between $[Fe(CN)_6]^{3-}$ and $[Fe(CN)_6]^{4-}$; these are catalysed by additional M^+, or the effect completely removed by the addition of suitable crown ethers.[54] The source of this effect is attributed to the collision or association of the $[Fe(CN)_6]^{3-/4-}$ anions with the M^+ cations, opening M^+-catalysed reaction pathways.[52] It is also sensitive to a number of other factors, such as viscosity, light, *etc.*[55,56]

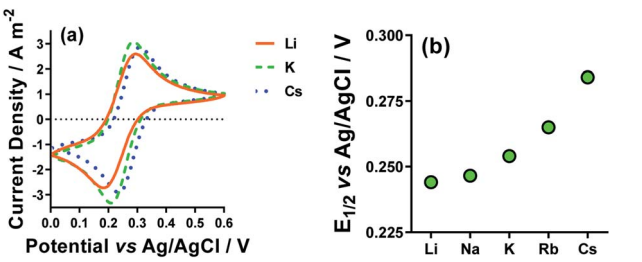

Fig. 6 Showing (a) Cyclic voltammograms (CVs) recorded for 5 mM $K_3[Fe(CN)_6]$ and 5 mM $K_4[Fe(CN)_6]$ in the presence of 0.4 M M_2SO_4 (M = Li^+ (orange solid line), K^+ (green dashed line) and Cs^+ (blue dotted line)) and (b) the trend in $E_{1/2}$ extracted from the CVs for all five alkali metal cations. All recorded at a Pt electrode at 50 mV s^{-1} and room temperature.

3.2.2 Cation effect upon the S_e of the $[Fe(CN)_6]^{3-}$/$[Fe(CN)_6]^{4-}$ redox couple. Next, the temperature dependence generated across two electrodes in the presence of a temperature gradient ($\Delta E/\Delta T$) was quantified for the various systems by measurement in a 2-electrode (both platinum) non-isothermal thermogalvanic cell. Since this is being investigated with respect to thermogalvanic systems, the temperature dependence upon the potential is referred to as the apparent Seebeck coefficient of the systems (S_e). Both cation and anion effects were assessed using 5 mM $K_3[Fe(CN)_6]$ and 5 mM $K_4[Fe(CN)_6]$ in the presence of 0.4 M M_2SO_4 (as above, where $M^+ : K^+$ is *ca.* 23 : 1). Additionally, M_2SO_4 was also substituted with 1 M MCl (where $M^+ : K^+$ is *ca.* 29 : 1).

The S_e values were determined by the gradient of the measured ΔE *vs.* ΔT (5 °C, 10 °C, 15 °C and 20 °C) for each of these systems; the corresponding ΔS_{rc} were then calculated using eqn (1). These results are summarised in Fig. 7, and show a general trend of increasing S_e values from $Li^+ < Na^+ < Rb^+ < Cs^+$, and also consistently higher S_e values in the MCl systems relative to the M_2SO_4 systems. The K^+ system was a notable outlier from the periodic trend, falling in the order: $Li^+ < \mathbf{K^+} < Na^+ < Rb^+ < Cs^+$.

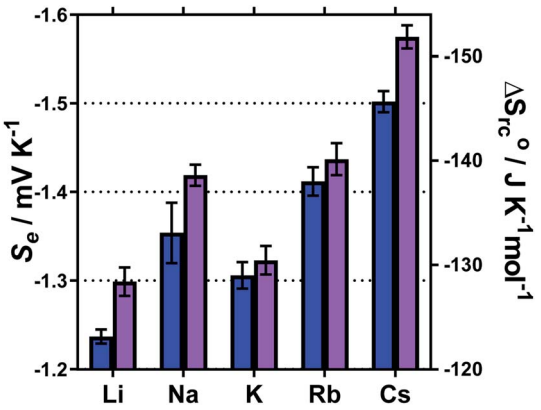

Fig. 7 Bar chart showing the measured S_e and calculated corresponding redox-couple entropy changes (ΔS_{rc}) for 5 mM of $K_3[Fe(CN)_6]$ and 5 mM $K_4[Fe(CN)_6]$ in the presence of either 0.4 M X_2SO_4 (blue) or 1 M XCl (purple) where X is shown as either Li, Na, K, Rb or Cs. All values determined using a non-isothermal platinum thermocell.

Recently, Huang *et al.* investigated similar systems but using isothermal cyclic voltammetry (hence reported dE°/dT rather than $\Delta E/\Delta T$) and observed the same trend as observed here for the $E_{1/2}$ (Fig. 6), namely that the S_e increased following the trend $Li^+ < Na^+ < K^+ < Rb^+ < Cs^+$.[43] In our case, the K^+ system did not fit into this trend, but K^+ is the only system to not contain a mixture of alkali metal cations; solutions containing two or more alkali metal cations are known to have significant effects upon the solvation dynamics of $[Fe(CN)_6]^{4-}$.[57]

Regarding the increase in S_e upon going from Li^+ to Cs^+, Huang *et al.* attributed this to the structure breaking and structure making nature of these cations, respectively.[43] However, observed variations in the S_e have more frequently been attributed to changes in the activity coefficients in line with Debye–Hückel electrostatic interactions.[16,30,46] This is consistent with the trend in activity coefficients, since M^+ systems are known to mirror the trend $Li^+ < Na^+ < K^+ < Rb^+ < Cs^+$.[58] Arguably, the structure making/breaking nature of the cations and extended Debye–Hückel theory reflects the same solvation dynamics, and therefore explains the same observations but from different perspectives.

3.2.3 Cation effect upon the thermogalvanic power of the $[Fe(CN)_6]^{3-}$/$[Fe(CN)_6]^{4-}$ redox couple. Next, having (re)evaluated the effect of M^+ upon the $E_{1/2}$ and S_e of the $[Fe(CN)_6]^{3-/4-}$ couple, its effect upon the current output (as short circuit current density, j_{sc}) and maximum power density output (P_{max}) was evaluated; this appears to be the first systematic evaluation of the effect of the cation upon the thermogalvanic properties of the $[Fe(CN)_6]^{3-/4-}$ couple.

Here Li^+, K^+ and Cs^+ were investigated, using 25 mM $K_3[Fe(CN)_6]$ and 25 mM $K_4[Fe(CN)_6]$ in the presence of 1.5 M of MCl; this had to be changed from the more dilute systems used above since the current in the dilute systems suffered from background noise and were therefore not suitably reproducible. The same trend in S_e was observed, and the j_{sc} increased going from Li^+ to K^+ to Cs^+ (shown by the linear I–V plots in Fig. 8(a)), and therefore P_{max} also followed the same trend (power curves in Fig. 8(a), and bar chart in Fig. 8(b)). Notably, going from Li^+ to Cs^+ the power doubled, indicating a significant electrocatalytic factor is introduced into the thermogalvanic cell by the nature of the alkali metal cation. This mirrors the reported investigations into the effect of these cations upon the apparent k^0 of the $[Fe(CN)_6]^{3-/4-}$ couple.[43,52,53]

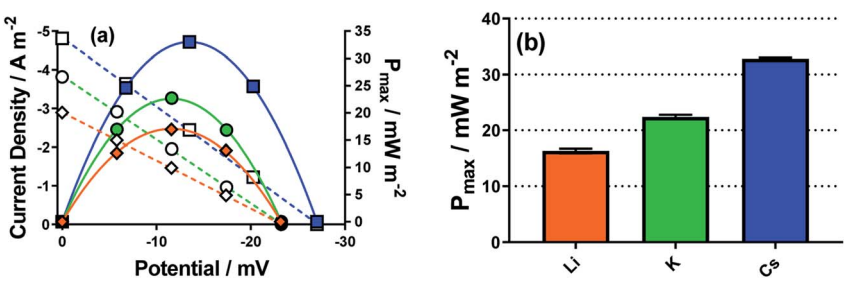

Fig. 8 Showing (a) representative I–V plots (hollow symbols) and power curves (filled symbols) for Cs^+ (blue square), K^+ (green circle) and Li^+ (orange diamond), and (b) bar chart summarising the effect of the dominant alkali metal cation on the P_{max}. All recorded for 25 mM $K_3[Fe(CN)_6]$, 25 mM $K_4[Fe(CN)_6]$ and 1.5 M of MCl in a non-isothermal thermogalvanic cell using platinum electrodes, with $\Delta T = 18$ °C ($T_{cold} = 17$ °C).

3.3. Thermogalvanic power *via* heterogeneous electrocatalysis

As demonstrated above, a homogeneous electrocatalytic effect was observed *via* added cations. It is also well established that the nature of the electrode material is highly influential upon the power generated by thermogalvanic cells (*i.e.* heterogeneous electrocatalysis).[33,39,59] Three electrode materials were therefore tested, as shown in Fig. 9(a), using equimolar 0.2 M $K_3[Fe(CN)_6]$ and 0.2 M $K_4[Fe(CN)_6]$. These were two forms of graphite, and platinum metal. Gold electrodes are known to experience passivation and dissolution issues with the $[Fe(CN)_6]^{3-/4-}$ redox couple,[34] and when tested here we were unable to obtain P_{max} values of sufficient reproducibility.

The platinum electrodes generated the highest average P_{max} value of 124 mW m^{-2} (Fig. 9), in line with expectations and previous reports.[33,39] Carbon electrodes have variable surface functionality and therefore variable electrocatalytic ability;[4] the two graphite electrodes tested here displayed significantly different P_{max} values (Fig. 9). One form of graphite, highly crystalline pyrolytic graphite (sold as a thermal interface sheet), gave a P_{max} of 36 mW m^{-2}, whereas amorphous graphite pressed into a sheet (sold as a gasket material) gave a P_{max} nearly 3 times higher, of 108 mW m^{-2}. This difference likely relates to the different forms of graphite at the surface; amorphous graphite is expected to have numerous edge-sites facing the solution, relative to the highly crystalline pyrolytic graphite, and such edge-sites are known to be more electrocatalytically active than basal planes for redox couples such as $[Fe(CN)_6]^{3-/4-}$.[60] These results were modelled using the modified Butler–Volmer equation (eqn (8) and (9)) and yielded the expected k_{agg} values, ranging from 0.58×10^{-4} cm s^{-1} for the crystalline graphite though to 1.93×10^{-4} cm s^{-1} for platinum (full values in Table S7 in the ESI†).

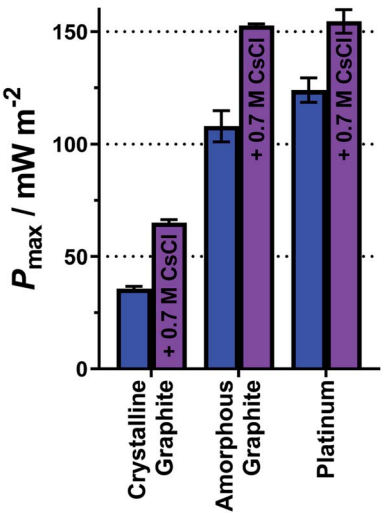

Fig. 9 Bar chart showing the P_{max} for 0.2 M $K_3[Fe(CN)_6]$ and 0.2 M $K_4[Fe(CN)_6]$ equimolar thermocell, using three different electrode materials; crystalline graphite, amorphous graphite and platinum, without (blue bars) and with (purple bars) 0.7 M CsCl present in the electrolyte. All measured at an applied $\Delta T = 18$ K ($T_{cold} = 17$ °C).

Finally, having investigated both homogeneous and heterogeneous electrocatalysis separately, they were also compared when combined. Fig. 9 displays the P_{max} values for the three electrode materials for just 0.2 M $K_3[Fe(CN)_6]$ and 0.2 M $K_4[Fe(CN)_6]$ (blue bars) as well as P_{max} after the addition of 0.7 M CsCl (purple bars). This system only had a ratio of 1 : 2 for $Cs^+ : K^+$, but could not be increased further due to solubility limitations. However, even this modest amount of Cs^+ significantly increased P_{max}, and this homogeneous electrocatalytic effect was observed across the three electrode materials; the P_{max} was boosted by *ca.* 80% at the highly crystalline pyrolytic graphite, and P_{max} increased by *ca.* 40% at the two (more heterogeneous electrocatalytic) electrodes. This was a result of more modest increases in the k_{agg} values, *e.g.* by 38% on the highly crystalline pyrolytic graphite, and by 25% on platinum.

3.4. A relative cost comparison of the different homogeneous systems

Finally, a preliminary economic assessment was made of the various homogeneous routes presented here as ways to increase thermogalvanic power output. The heterogeneous electrocatalytic aspects (*i.e.* platinum *vs.* graphite) were not considered because bulk materials were employed, but numerous other approaches could be employed to minimise the amount of material utilised (*e.g.* sputtering of a thin film of platinum).[13]

Fig. 10(a) summarises the maximum power density outputs from the equimolar 0.2 M $K_3[Fe(CN)_6]$ and 0.2 M $K_4[Fe(CN)_6]$ amorphous graphite cell, against the same cell but with non-equimolar ratios, and the same cell with 0.7 M CsCl. Fig. 10(b) (grey bars) displays the power normalised with respect to the cost of the salt dissolved in the solution (assuming Sigma Aldrich *ReagentPlus* grade materials utilised; full details in ESI†), whereby the equimolar cell has been set to a cost per W m^{-2} of 1. What is clearly observed is that while the addition of CsCl increased the overall power (Fig. 10(a)), the significantly higher cost of CsCl resulted in an 685% increase in cost per W m^{-2} (Fig. 10(b), purple bar). Conversely, because *ReagentPlus* $K_4[Fe(CN)_6]$ was *ca.* 22% cheaper per mol than *ReagentPlus* $K_3[Fe(CN)_6]$, and having more $K_4[Fe(CN)_6]$ generated more power, moving away from the 0.2 M stoichiometric ratio commonly employed by others can actually result in a decrease in cost per W m^{-2}; this reaches an optimum at 0.10 M $K_3[Fe(CN)_6]$ and 0.30 M $K_4[Fe(CN)_6]$, at only 92% of the cost per W m^{-2} of the equimolar system. However, an important caveat is that this only applies at current prices and using 0.5 kg bottles of *ReagentPlus* grade materials; the relative cost of $K_4[Fe(CN)_6]$ and $K_3[Fe(CN)_6]$ actually invert for *ACS grade* material (Fig. 10(b), red bars), thereby making the 0.25 M $K_3[Fe(CN)_6]$ and 0.15 M $K_4[Fe(CN)_6]$ cell have the lowest cost per W m^{-2}, by a modest 1% relative to the equimolar cell.

While the reductions in cost per W m^{-2} are modest, both nevertheless demonstrate that a 'less is more', non-stoichiometric approach can be viable for thermogalvanic

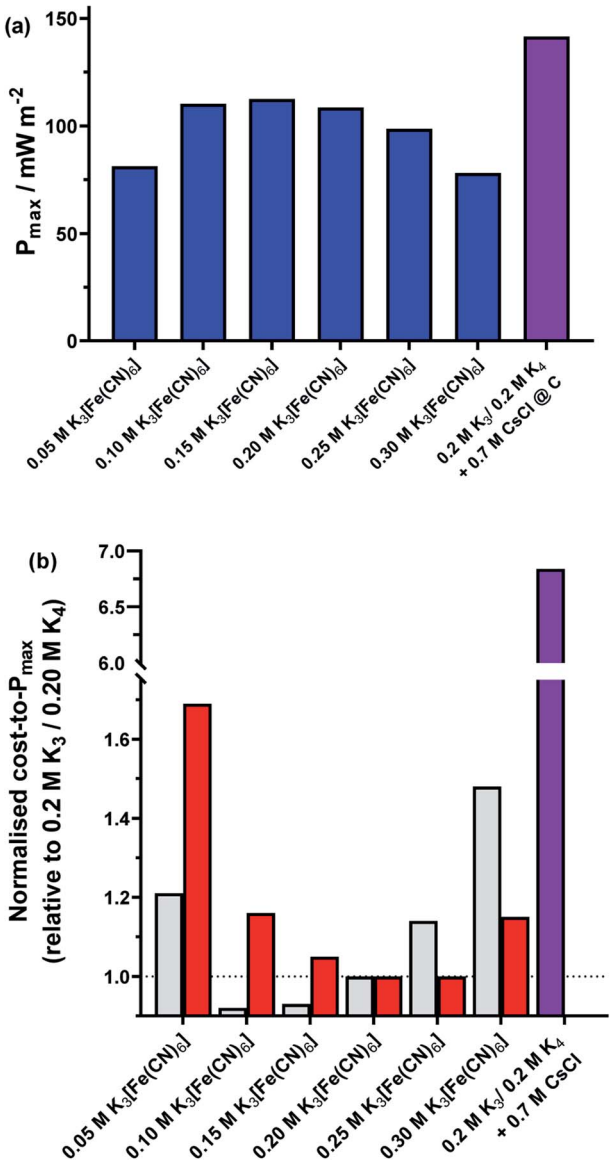

Fig. 10 Plots of the (a) P_{max} produced by the 0.4 M $K_{3/4}[Fe(CN)_6]$ thermocells at non-equimolar ratios (blue bars) and the equimolar ratio in the presence of 0.7 M CsCl (purple bar). Also shown is (b) the trend in electrolyte cost-to-P_{max} for each of these systems, normalised with respect to the equimolar 0.2 M $K_3[Fe(CN)_6]$ and 0.2 M $K_4[Fe(CN)_6]$ system. This is shown for *ReagentPlus* grade $K_{3/4}[Fe(CN)_6]$ (grey bars) and *ACS* grade $K_{3/4}[Fe(CN)_6]$ (red bars); the significantly higher cost for *ReagentPlus* grade 0.4 M $K_{3/4}[Fe(CN)_6]$ and *ReagentPlus* grade 0.7 M CsCl is also shown (purple bar; please note scale break on the *y*-axis). All power values measured at amorphous graphite electrodes, and an applied $\Delta T = 18$ °C ($T_{cold} = 17$ °C).

cells from a technoeconomic perspective. Clearly both good heterogeneous and homogeneous electrocatalysts are required to achieve the highest power cells, but what is demonstrated here is that the deliberate addition of additives that are significantly more costly than the redox active species themselves are hard to justify economically, unless even more significant increases in P_{max} can be achieved.

4. Conclusions

This research set out to explore some fundamental aspects of thermogalvanic cells, using ferricyanide/ferrocyanide as a 'standard' redox couple. By comparing a standard concentration study using equimolar ratios with apparently the first systematic study of non-equimolar ratios, significant insight was generated. This demonstrated how the Seebeck coefficient is concentration dependent (*via* Debye–Hückel theory, in line with prior observations) and is even more significantly sensitive to the ratio of ferricyanide to ferrocyanide (*via* the Nernst equation); it also allowed us to apply a slightly modified Butler–Volmer equation to quantitatively model the current and electrical power generated by the various systems. This Butler–Volmer model generated just one variable as an aggregated rate constant, k_{agg}.

Homogeneous electrocatalysis (the deliberate addition of an alkali metal salt to the electrolyte solution) was also explored alongside a more conventional heterogeneous electrocatalytic (electrode material) study. Both had significant effects upon the overall current produced by the thermocells, but homogeneous electrocatalysis could also boost the potential difference, by virtue of altered thermodynamics. Combining both optimal heterogeneous and homogeneous electrocatalysis generated the highest power thermocells. However, while addition of the alkali metal salt CsCl significantly boosted power (up to +80%), it increased the relative cost of the electrolyte by an even more significant margin (+685%). It was also demonstrated that moving from a standard equimolar system to a non-equimolar system could yield a higher maximum power (+4%), and could decrease the cost-per-unit-power of the thermocell electrolyte even more significantly (−8%).

These results help rationalise variations in thermocell performance as a function of concentration and ratio. It also introduces a means to quantitatively model the resulting performance to yield a single value as a performance metric, the k_{agg}.

Conflicts of interest

There are no conflicts to declare.

Acknowledgements

MAB acknowledges the EPSRC for funding (Standard Research Studentship (DTP), EP/N509498/1). LA and CJB acknowledges the PLuS Alliance for funding (PLuS Alliance Seed Grant, project code PA17046). HXL acknowledges the Chinese Scholarship Council for funding (CSC No. 201806130204).

References

1 P. Gründler, *In-situ Thermoelectrochemistry: Working with Heated Electrodes*, Springer, Berlin, 1st edn, 2015.
2 T. I. Quickenden and Y. Mua, *J. Electrochem. Soc.*, 1995, **142**, 3985–3994.

3 A. Gunawan, C. H. Lin, D. A. Buttry, V. Mujica, R. A. Taylor, R. S. Prasher and P. E. Phelan, *Nanoscale Microscale Thermophys. Eng.*, 2013, **17**, 304–323.
4 M. S. Romano, J. M. Razal, D. Antiohos, G. G. Wallace and J. Chen, *J. Nanosci. Nanotechnol.*, 2015, **15**, 1–14.
5 M. Dupont, D. R. MacFarlane and J. M. Pringle, *Chem. Commun.*, 2017, **53**, 6288–6302.
6 B. Burrows, *J. Electrochem. Soc.*, 1976, **123**, 154–159.
7 M. A. Buckingham, F. Marken and L. Aldous, *Sustainable Energy Fuels*, 2018, **2**, 2717–2726.
8 J. R. Sootsman, D. Y. Chung and M. G. Kanatzidis, *Angew. Chem., Int. Ed.*, 2009, **48**, 8616–8639.
9 H. Julian Goldmid, *Introduction to Thermoelectricity*, Springer Berlin Heidelberg, 2nd edn, 2016.
10 M. A. Buckingham and L. Aldous, *J. Electroanal. Chem.*, 2020, DOI: 10.1016/j.jelechem.2020.114280.
11 T. J. Abraham, D. R. Macfarlane and J. M. Pringle, *Energy Environ. Sci.*, 2013, **6**, 2639–2645.
12 T. J. Abraham, D. R. MacFarlane, R. H. Baughman, N. Li, Y. Chen and J. M. Pringle, *Mater. Res. Soc. Symp. Proc.*, 2019, **53**, 1689–1699.
13 M. Al Maimani, J. J. Black and L. Aldous, *Electrochem. Commun.*, 2016, **72**, 181–185.
14 C. Lin, A. Gunawan, P. E. Phelan, D. A. Buttry, V. Mujica, R. A. Taylor and R. S. Prasher, *Proc. ASME 2012 Int. Mech. Eng. Congr. Expo.*, 2012, vol. 1, pp. 1–7.
15 H. Li, A. Gunawan, P. E. Phelan, D. A. Buttry, V. Mujica, R. A. Taylor and R. S. Prasher, *Proc. ASME 2013 Int. Mech. Eng. Congr. Expo.*, 2013, vol. 1, pp. 1–2.
16 J. J. Black, T. Murphy, R. Atkin, A. Dolan and L. Aldous, *Phys. Chem. Chem. Phys.*, 2016, **18**, 20768–20777.
17 J. J. Black, A. Dolan, J. B. Harper and L. Aldous, *Phys. Chem. Chem. Phys.*, 2018, **20**, 16558–16567.
18 L. Aldous, J. J. Black, M. C. Elias, B. Gélinas and D. Rochefort, *Phys. Chem. Chem. Phys.*, 2017, **19**, 24255–24263.
19 E. H. B. Anari, M. Romano, W. X. Teh, J. J. Black, E. Jiang, J. Chen, T. Q. To, J. Panchompoo and L. Aldous, *Chem. Commun.*, 2016, **52**, 745–748.
20 H. Zhou, T. Yamada and N. Kimizuka, *J. Am. Chem. Soc.*, 2016, **138**, 10502–10507.
21 T. J. Abraham, D. R. MacFarlane and J. M. Pringle, *Chem. Commun.*, 2011, **47**, 6260–6262.
22 P. H. Daum and C. G. Enke, *Anal. Chem.*, 1969, **41**, 653–656.
23 R. L. McCreery, *Chem. Rev.*, 2008, **108**, 2646–2687.
24 E. L. Yee and M. J. Weaver, *Inorg. Chem.*, 1980, **19**, 1077–1079.
25 L. Zhang, T. Kim, N. Li, T. J. Kang, J. Chen, J. M. Pringle, M. Zhang, A. H. Kazim, S. Fang, C. Haines, D. Al-Masri, B. A. Cola, J. M. Razal, J. Di, S. Beirne, D. R. MacFarlane, A. Gonzalez-Martin, S. Mathew, Y. H. Kim, G. Wallace and R. H. Baughman, *Adv. Mater.*, 2017, **29**, 1605652.
26 T. Ikeshoji and R. S. Gonçalves, *J. Appl. Electrochem.*, 1993, **23**, 516–519.
27 T. Ikeshoji, *Bull. Chem. Soc. Jpn.*, 1987, **60**, 1505–1514.
28 R. Hu, B. A. Cola, N. Haram, J. N. Barisci, S. Lee, S. Stoughton, G. Wallace, C. Too, M. Thomas, A. Gestos, M. E. Dela Cruz, J. P. Ferraris, A. A. Zakhidov and R. H. Baughman, *Nano Lett.*, 2010, **10**, 838–846.
29 H. Im, T. Kim, H. Song, J. Choi, J. S. Park, R. Ovalle-Robles, H. D. Yang, K. D. Kihm, R. H. Baughman, H. H. Lee, T. J. Kang and Y. H. Kim, *Nat. Commun.*, 2016, **7**, 10600.
30 T. J. Kang, S. Fang, M. E. Kozlov, C. S. Haines, N. Li, Y. H. Kim, Y. Chen and R. H. Baughman, *Adv. Funct. Mater.*, 2012, **22**, 477–489.
31 M. S. Romano, N. Li, D. Antiohos, J. M. Razal, A. Nattestad, S. Beirne, S. Fang, Y. Chen, R. Jalili, G. G. Wallace, R. Baughman and J. Chen, *Adv. Mater.*, 2013, **25**, 6602–6606.
32 F. Zhao, W. Qian, M. Li, W. Li, L. Chen, F. Zhong, W. Huang and C. Dong, *RSC Adv.*, 2017, **7**, 23890–23895.
33 H. A. H. Alzahrani, J. J. Black, D. Goonetilleke, J. Panchompoo and L. Aldous, *Electrochem. Commun.*, 2015, **58**, 76–79.
34 H. A. H. Alzahrani, M. A. Buckingham, F. Marken and L. Aldous, *Electrochem. Commun.*, 2019, **102**, 41–45.
35 H. Im, H. G. Moon, J. S. Lee, I. Y. Chung, T. J. Kang and Y. H. Kim, *Nano Res.*, 2014, **7**, 443–452.
36 W. Huang, J. Xu, K. He, Z. Li, W. Qian and C. Dong, *IOP Conf. Ser. Earth Environ. Sci.*, 2018, **121**, 042027.
37 N. E. Holubowitch, J. Landon, C. A. Lippert, J. D. Craddock, M. C. Weisenberger and K. Liu, *ACS Appl. Mater. Interfaces*, 2016, **8**, 22159–22167.
38 M. S. Romano, S. Gambhir, J. M. Razal, A. Gestos, G. G. Wallace and J. Chen, *J. Therm. Anal. Calorim.*, 2012, **109**, 1229–1235.
39 J. Wu, J. J. Black and L. Aldous, *Electrochim. Acta*, 2017, **225**, 482–492.
40 T. Kim, J. S. Lee, G. Lee, H. Yoon, J. Yoon, T. J. Kang and Y. H. Kim, *Nano Energy*, 2017, **31**, 160–167.
41 D. Inoue, Y. Fukuzumi and Y. Moritomo, *Jpn. J. Appl. Phys.*, 2020, **59**, 037001.
42 J. Duan, G. Feng, B. Yu, J. Li, M. Chen, P. Yang, J. Feng, K. Liu and J. Zhou, *Nat. Commun.*, 2018, **9**, 1–8.
43 B. Huang, S. Muy, S. Feng, Y. Katayama, Y. C. Lu, G. Chen and Y. Shao-Horn, *Phys. Chem. Chem. Phys.*, 2018, **20**, 15680–15686.
44 L. Jin, G. W. Greene, D. R. MacFarlane and J. M. Pringle, *ACS Energy Lett.*, 2016, **1**, 654–658.
45 P. Yang, K. Liu, Q. Chen, X. Mo, Y. Zhou, S. Li, G. Feng and J. Zhou, *Angew. Chem., Int. Ed.*, 2016, **55**, 12050–12053.
46 M. Bonetti, S. Nakamae, M. Roger and P. Guenoun, *J. Chem. Phys.*, 2011, **134**, 114513–114518.
47 P. Blanc and C. Madic, *Inorg. Chim. Acta*, 1984, **94**, 134–136.
48 A. J. Bard and L. R. Faulkner, *Electrochemical Methods: Fundamentals and Applications*, John Wiley & Sons, Inc., 2nd edn, 2001.
49 K. Winkler, *J. Electroanal. Chem.*, 1995, **388**, 151–159.
50 D. H. Angell and T. Dickinson, *J. Electroanal. Chem.*, 1972, **35**, 55–72.
51 J. M. Hornut and A. Storck, *J. Appl. Electrochem.*, 1991, **21**, 1103–1113.
52 L. M. Peter, W. Dürr, P. Bindra and H. Gerischer, *J. Electroanal. Chem.*, 1976, **71**, 31–50.

53 S. A. Campbell and L. M. Peter, *J. Electroanal. Chem.*, 1994, **364**, 257–260.
54 A. Zahl, R. Van Eldik and T. W. Swaddle, *Inorg. Chem.*, 2002, **41**, 757–764.
55 D. E. Khoshtariya, T. D. Dolidze, A. Neubrand and R. Van Eldik, *J. Mol. Liq.*, 2000, **89**, 127–146.
56 D. E. Khoshtariya, T. D. Dolidze, D. Krulic, N. Fatouros and D. Devilliers, *J. Phys. Chem. B*, 1998, **102**, 7800–7806.
57 A. J. Esswein, J. Goeltz, D. Amadeo, High solubility iron hexacyanides, US 2014/0051003 A1, 2014, p. 14.
58 A. Salis and B. W. Ninham, *Chem. Soc. Rev.*, 2014, **43**, 7358–7377.
59 T. J. Abraham, N. Tachikawa, D. R. MacFarlane and J. M. Pringle, *Phys. Chem. Chem. Phys.*, 2014, **16**, 2527–2532.
60 C. E. Banks, M. R. Moore, T. J. Davies and R. G. Compton, *Chem. Commun.*, 2004, **10**, 1804–1805.